

DOTA: A Dynamically-Operated Photonic Tensor Core for Energy-Efficient Transformer Accelerator

Hanqing Zhu¹, Jiaqi Gu^{1,3}, Hanrui Wang², Zixuan Jiang¹,
Zhekai Zhang², Rongxing Tang¹, Chenghao Feng¹,
Song Han², Ray T. Chen¹, David Z. Pan¹

¹The University of Texas at Austin,

²Massachusetts Institute of Technology, ³Arizona State University

ABSTRACT

The wide adoption and significant computing resource consumption of attention-based Transformers, e.g., Vision Transformer and large language models, have driven the demands for efficient hardware accelerators. While electronic accelerators have been commonly used, there is a growing interest in exploring photonics as an alternative technology due to its high energy efficiency and ultra-fast processing speed. Optical neural networks (ONNs) have demonstrated promising results for convolutional neural network (CNN) workloads that only require weight-static linear operations. However, they fail to efficiently support Transformer architectures with attention operations due to the lack of ability to process dynamic full-range tensor multiplication. In this work, we propose a customized high-performance and energy-efficient photonic Transformer accelerator, DOTA. To overcome the fundamental limitation of existing ONNs, we introduce a novel photonic tensor core, consisting of a crossbar array of interference-based optical vector dot-product engines, that supports highly-parallel, dynamic, and full-range matrix-matrix multiplication. Our comprehensive evaluation demonstrates that DOTA achieves a $>4\times$ energy and a $>10\times$ latency reduction compared to prior photonic accelerators, and delivers over $20\times$ energy reduction and 2 to 3 orders of magnitude lower latency compared to the electronic Transformer accelerator. Our work highlights the immense potential of photonic computing for efficient hardware accelerators, particularly for advanced machine learning workloads.

1. INTRODUCTION

In recent years, attention-based Transformers have gained immense popularity and demonstrated remarkable success in various domains such as natural language processing (NLP) [5, 22, 32] and computer vision (CV) tasks [8, 13, 46]. The attention mechanism employed in Transformers enables dynamic feature aggregation, long-distance modeling, and global context extraction, contributing significantly to their impressive performance [13, 47]. However, this exceptional performance comes at a considerable computational cost. The quadratic complexity of attention modules, both in terms of computation and memory, combined with a large number of parameters, demands substantial computational resources. This poses a challenge for deploying Transformers, particularly in resource-constrained systems where such computational demands are prohibitive. To address this challenge,

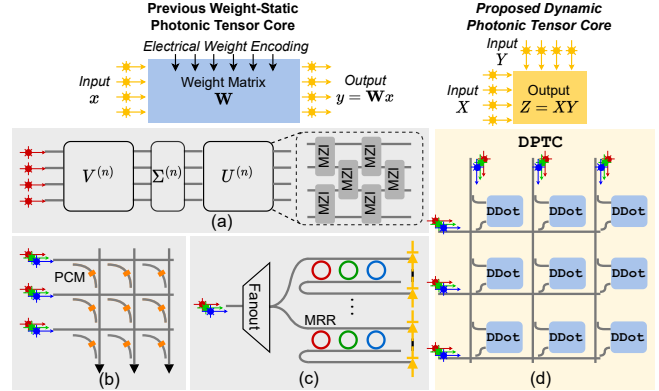


Figure 1: (a), (b), (c) Previous weight-static photonic tensor core designs [15, 40, 44]. (d) Our proposed dynamic photonic tensor core.

there is a pressing need to develop domain-specific hardware accelerators for the efficient deployment of Transformers in real-world applications.

Several hardware accelerators based on digital electronics have been proposed to accelerate the inference of Transformers [11, 42, 49, 52, 55]. However, traditional electrical digital computing platforms face significant challenges as transistor-based chips reach the limits of Dennard scaling. This has led to increased power dissipation per unit area and diminishing performance improvements. As a compelling alternative, integrated optical neural networks (ONNs) have emerged as next-generation computation platforms offering ultra-high speed, high parallelism, and low energy consumption. Various optical systems are actively being studied for accelerating convolutional neural network (CNN) workloads, e.g., Mach-Zehnder interferometer (MZI) arrays [40], Micro-ring Resonator (MRR)-based ONNs [43, 44], and non-volatile Phase Change Material (PCM)-based crossbar [15].

However, existing photonic accelerators are mainly designed and optimized for weight-static NNs, e.g., CNNs, where convolution and fully-connected layers only involve matrix multiplications (MM) between the learned weight matrix and input tensors. They fail to efficiently support attention-based Transformers due to the following *challenges*.

Matrix multiplication with two dynamic input operands. Unlike digital electronics, prior photonic tensor cores (PTC) typically preload and encode one operand of MM (usually the weight matrix \mathbf{W}) onto the circuit transmission, shown in Figure 1. This procedure usually involves high costs in weight

mapping and device programming. For example, the MZI array [40] requires singular value decomposition (SVD) and phase decomposition for matrix mapping. To map a 12×12 matrix, the required time for SVD and phase decomposition on CPU is ~ 1.5 ms. Moreover, those PTC designs prefer to use lowloss, compact, and non-volatile devices that usually cost $10ns - 10\mu s$ to be programmed [3, 15, 35]. Attention in Transformers is built on matrix multiplication between two dynamically generated activations, which requires both weight mapping and device programming be performed at runtime. Frequent remapping and reprogramming are generally not affordable or easily amortized given their orders-of-magnitude higher runtime cost than ultra-fast computing (< 100 ps). MRR-based tensor cores using high-speed modulators can intrinsically support dynamic matrix-vector multiplication (MVM) without complicated weight mapping, but its energy efficiency is limited by the high modulation cost.

Matrix multiplication with full-range input operands. Prior incoherent PTCs pose range limitations on operands. At least one of the operands is limited to be only non-negative due to their intrinsic magnitude/intensity modulation and detection mechanism. However, Transformers require full-range matrix multiplications. The absence of full range support often requires decomposing full-range operands into differences of non-negative operands ($X_+ - X_-$)($Y_+ - Y_-$) and processing X_+Y_+ , X_+Y_- , X_-Y_+ , and X_-Y_- separately [3, 43] with additional accumulation steps, incurring $2-4 \times$ hardware cost compared to one that supports full-range operands.

Above all, existing photonic accelerators encounter significant difficulties in efficiently realizing the dynamic full-range MM workloads inherent in Transformers. To address those challenges, in this work, we propose the *first* customized photonic accelerator to support attention-based Transformer models, which we refer to as DOTA. In DOTA, we first design a dot-product engine DDot that enables multiplication between two dynamically encoded full-range optical vectors. DDot directly encodes full-range dynamic input operands as high-speed coherent optical signals, thus can represent signs as the signal phases and support real-time operand switching with negligible mapping or programming cost (< 10 ps). Furthermore, the dot-product mechanism is based on coherent light interference with a coupler and balanced photodetection, which further enables to detect full-range dot-product results as positive or negative photocurrent. Based on DDot, we devise a novel dynamically-operated photonic tensor core, DPTC for ultra-parallel and energy-efficient dynamic full-range matrix multiplication, which is the key building block of our photonic Transformer accelerator. We fully leverage both spectral and spatial parallelism of optics by exploiting the wavelength-division multiplexing (WDM) capacity and on-chip optical broadcast. As a result, we can maximize the hardware sharing, trim input modulation overhead, and significantly boost processing parallelism and efficiency.

The major contributions of this paper are as follows:

- We present, *for the first time*, a customized energy-efficient photonic Transformer accelerator, DOTA, overcoming the efficiency and flexibility limitations of existing photonic accelerators for Transformer acceleration.
- We design a novel dynamically-operated photonic ten-

sor core, DPTC, that enables ultra-parallel and energy-efficient dynamic full-range general matrix multiplication in a one-shot way. DPTC harnesses both spectral and spatial parallelism of optics by utilizing WDM and on-chip optical broadcast to maximize hardware sharing and operand sharing, offering exceptional processing parallelism and energy efficiency.

- We comprehensively evaluate our proposed DOTA compared to previous photonic and electronic accelerator designs across different Transformer benchmarks. Our DOTA significantly outperforms prior photonic designs, achieving a $> 4 \times$ energy reduction and a $> 10 \times$ computation latency decrease. Furthermore, compared to the current state-of-the-art electronic Transformer accelerators, DOTA delivers over $20 \times$ energy reduction and achieves 2 to 3 orders of magnitude lower latency.

2. PRELIMINARIES AND BACKGROUND

2.1 Transformer and Self-Attention

Transformer [47] was initially proposed as a sequence transduction model for natural language processing tasks. Three mainstream Transformer architectures are encoder-decoder (BERT [22], ViT [13]), causal decoder (GPT-series [6, 36, 37]), and the prefix decoder (GLM-130B [53]). In spite of the difference among the Transformer architectures, these models are usually a stack of several identical blocks. Both encoder and decoder blocks mainly comprise a multi-head self-attention (MHA) module, a feed-forward network (FFN), the shortcut connection, and layer normalization. Decoder additionally inserts cross-attention and masked self-attention modules. We use the basic encoder block as an example, which is defined by the following equations.

$$\begin{aligned} \mathbf{X}'_{l+1} &= \text{MHA}(\text{LN}(\mathbf{X}_l)) + \mathbf{X}_l \\ \mathbf{X}_{l+1} &= \text{FFN}(\text{LN}(\mathbf{X}'_{l+1})) + \mathbf{X}'_{l+1} \end{aligned} \quad (1)$$

where \mathbf{X}_l is input sequences of l -th layer. Layer normalization (LN) [4] is applied prior to the MHA and FFN modules.

Multi-head Self-Attention (MHA). Attention is the novel feature of Transformers where the pairwise correlations across the entire input sequence are computed. Each MHA has H self-attention heads. In each head, the input vector is first transformed into the query (Q), key (K), and value (V) vectors by linear projection. Then, the attention function between different input vectors is computed as,

$$\text{Attention}(\mathbf{Q}, \mathbf{K}, \mathbf{V}) = \text{softmax}\left(\frac{\mathbf{Q}\mathbf{K}^T}{\sqrt{d_k}}\right)\mathbf{V}, \quad (2)$$

where d_k is Q and K 's dimension. The outputs of all heads are concatenated together and then passed through a linear projection. Notably, attention is totally different from the linear layer, which poses unique challenges for the inference accelerator. In a linear layer, the matrix multiplication is conducted between the static weight matrix and the dynamic input matrix. On the contrary, attention requires the matrix multiplication between dynamically generated matrices, i.e., Q , K , and V .

Feed-forward Network (FFN). The FFN module usually consists of two dense linear layers with a non-linear activation

Table 1: Comparison to prior ONNs. Each ONN takes two operands to perform either matrix-vector multiplication (MVM) or matrix-matrix multiplication (MM). Previous approaches have suffered from (1) complicated weight mapping or severe operand programming overhead and (2) limitations on operand range.

ONN Designs	MZI arrays [40]	MRR ONN 1 [44]	MRR ONN 2 [43]	PCM Photonic Crossbar [15]	Ours DOTA
Operand 1	Static, Full-range	Dynamic, Full-range	Dynamic, Positive Only	Static, Positive Only	Dynamic, Full-range
Operand 2	Dynamic, Full-range	Dynamic, Positive Only	Dynamic, Positive Only	Dynamic, Positive Only	Dynamic, Full-range
Dynamic-operand Op.	No	Yes	Yes	No	Yes
Mapping & Programming Cost	High	Medium	High	Low	Low
Operation Type	MVM	MVM	MVM	MM	MM

function in between. The GELU activation function [20] is a popular option compared to other activation functions, providing better performance and full-range output.

2.2 Optical Computing Basics

To enable photonic computing, photonic tensor cores are constructed by cascading basic optical devices.

Phase shifter (PS): PS is an active device that can produce a controlled phase shift ϕ on the propagating light signal x by manipulating the effective refractive index of waveguides. The resulting output is $e^{j\phi}x$.

Directional coupler (DC): DC is a passive device that can produce interference between two coherent light signals. Its transfer matrix of a 2-by-2 DC is $\begin{bmatrix} t & \sqrt{1-t^2}j \\ \sqrt{1-t^2}j & t \end{bmatrix}$, where $t \in [0, 1]$ is the transmission coefficient. Usually, we set $t = \sqrt{2}/2$ as a 3 dB 50:50 DC.

Mach-Zehnder Modulator (MZM): MZM starts with one splitter that splits the optical input E_{in} into upper and lower modulator arms. After being phase modulated, the signals from the two arms are recombined as the optical output E_{out} . With equal splitting and differential phase shift, $+\phi$ and $-\phi$ on the two arms [24], respectively, full-range encoding $E_{out} = E_{in} \cos \phi$ can be achieved with MZM by tuning $\phi \in [0, \pi]$.

Microring/microdisk resonator: Micro-ring (MRR) and microdisk (MD) resonators are compact photonic devices that serve as narrowband filters to enable the transmission of a certain wavelength. They can be utilized for constructing optical switches and WDM MUX and DEMUX units.

Mach-Zehnder interferometer (MZI): MZI consists of two cascaded directional couplers and two phase shifters. It can perform arbitrary 2-D unitary matrix operations, thus serving as a basic building block for constructing MZI-based PTCs [40] with the concern of a large device footprint.

2.3 Challenges of Prior ONNs for Transformer

Some ONNs [16, 17, 56] are customized to only support sub-space linear operations with restricted matrix expressivity for higher efficiency. Due to their inability to express arbitrary matrices, we omit the discussion of subspace PTCs and focus on universal linear units that can potentially support attention operations, e.g., MZI arrays [40], MRR-based ONNs [43, 44], and non-volatile PCM-based crossbar [15].

Table 1 compares prior photonic accelerators' operand mapping and programming characteristics and operation type (MM or MVM). They are mainly designed and optimized for weight-static NN architectures and are inclined towards a low refresh rate of one operand (typically the static weight matrix). As a result, they struggle to efficiently support attention-based Transformers due to Transformers' unique characteristics.

The primary challenge lies in supporting **matrix multiplication with two dynamic input operands**, a crucial requirement in attention modules. To clarify, we define the concepts of *dynamic* and *static* operands. In the GEMM for attention operations, both operands are intermediate input-dependent activations generated in real-time, rendering them dynamic. In contrast, weight matrices in convolutional or linear layers, remain fixed throughout the inference process, making them static. Prior ONNs typically preload and encode the static operand of MM (usually the weight matrix \mathbf{W}) onto the circuit transmission, which usually involves high costs in weight mapping and device programming. This feature makes them more suitable for weight-static applications, resulting in a typical adoption of a "weight-stationary" dataflow. For instance, MZI array [40] requires SVD and phase decomposition for matrix mapping, which can take around ~ 1.5 ms to obtain the required phase information on a CPU for a 12×12 matrix. Furthermore, current optical neural networks (ONNs) face challenges in terms of bulky area and significant insertion loss. Consequently, these ONNs tend to favor low-loss, compact, and non-volatile devices. However, these devices suffer from slow programming times, ranging from 10 ns to 10 μ s. When applied to dynamic MMs in attention, the weight mapping and device programming for operands must be carried out at runtime during inference. This becomes impractical as the programming times are orders of magnitude slower than the ultra-fast computing required (< 100 ps), resulting in severe system stalls. The MRR-based ONNs can support dynamic matrix multiplication via direct weight mapping using high-speed modulators and DACs. However, these MRR-based ONNs either have only one operand broadcast [44] or lack operand broadcast [43], leading to significant modulation costs without optimized sharing, which ultimately restricts energy efficiency.

Another significant requirement for Transformers is the need for **MM with full-range input operands**, as activations are not restricted to non-negative values only. This is especially true with the widespread utilization of activation functions such as GELU and LayerNorm across Transformer layers. However, previous ONNs impose limitations on operand ranges.

In prior incoherent ONNs, at least one operand of MMs is constrained to be non-negative due to the intrinsic magnitude/intensity modulation and detection mechanism. The absence of support for full-range operands/results often necessitates separate multiplications between positive and negative components, accompanied by additional partial product accumulation [3, 43]. This approach incurs a hardware cost that is 2-4 times higher compared to full-range PTCs.

Considering these challenges, existing ONNs are ill-equipped

to efficiently handle dynamic MM workloads in Transformers. Consequently, there is an urgent need for a dedicated design of PTCs that can enable energy-efficient acceleration of Transformers using photonics.

3. PROPOSED NEW PHOTONIC DESIGN

To efficiently support attention-based Transformers using photonics, it is crucial to have a customized design instead of merely adopting previous weight-static photonic tensor cores. The new photonic design must possess three essential traits:

- Support for **general matrix multiplications**.
- Efficient handling of **dynamic operands with low encoding and signal modulation cost**.
- Support for **full-range inputs/outputs**.

To meet these requirements, we propose our photonic accelerator design, starting with the foundational dynamic-operated dot-product engine, DDot , which is capable of computing the dot-product two dynamically encoded full-range optical vectors. Leveraging the capabilities of DDot , we then introduce our photonic tensor core design, DPTC , which enables highly parallel general matrix multiplication with low encoding and modulation overhead.

3.1 DDot : Dynamically-Operated Dot-Product Engine

To support MM between dynamic input operands, it is essential to have a design that supports a straightforward operand mapping scheme and high-speed device programming. Motivated by the design in [18], we introduce a dynamic optical dot-product engine called DDot , based on coherent light interference. Figure 2(a) depicts the structure of the optical dot-product engine that computes the dot product between two optical signals or vectors \mathbf{x} and \mathbf{y} . Unlike previous ONNs where one operand is mapped onto the circuit transmission that may need the extra operand decomposition step, our design directly encodes full-range dynamic input operands as high-speed coherent optical signals using Mach-Zehnder modulators (MZMs). Specifically, each pair of elements x_i and y_i in the two vectors is encoded in the light magnitude and phase at a unique wavelength. As discussed in Section 2.2, given the input light E_{in} with a magnitude of 1, the electric field at the output port of MZM is expressed as,

$$E_{out} = E_{in} \cos \theta, \quad (3)$$

which allows for a full encoding range of $[-1, 1]$ by tuning $\theta \in [0, \pi]$ to change the MZM transmission. The coherent interference mechanism in DDot enables the representation of sign information using the signal phases. In this work, we assume using MZM with a linear response, where the modulated output is proportional to the modulation power.

To perform optical multiplication, we leverage the directional coupler (DC) to enable coherent light interference. In DDot , we put a $-\pi/2$ phase shifter (PS) on the upper left port of a 50 : 50 DC shown in Figure 2(a). By shining the light signal carrying x_i and y_i through the proposed photonic engine, the outputs at the right and left output ports of the

DC, z_i^0 and z_i^1 can be computed as,

$$\begin{pmatrix} z_i^0 \\ z_i^1 \end{pmatrix} = \frac{1}{\sqrt{2}} \begin{pmatrix} 1 & j \\ j & 1 \end{pmatrix} \begin{pmatrix} 1 & 0 \\ 0 & e^{-j\frac{\pi}{2}} \end{pmatrix} \begin{pmatrix} x_i \\ y_i \end{pmatrix} = \frac{1}{\sqrt{2}} \begin{pmatrix} x_i + y_i \\ j(x_i - y_i) \end{pmatrix}. \quad (4)$$

The two output signals are orthogonal in the complex plane.

By adopting broadband devices in this proposed architecture, we can have the same transfer function for a range of wavelengths. Furthermore, by utilizing the wavelength-division multiplexing (WDM) technique, multi-wavelength signals can propagate concurrently on the same waveguide using a WDM multiplexer. In this way, with WDM signals, \mathbf{x} and \mathbf{y} , passing through this architecture, input pairs (x_i, y_i) encoded in the same wavelength interfere with each other in parallel following Eq. (4), while different optical wavelengths do not interfere. Photo-diode (PD) at the end of each output port of DC converts the incident WDM optical signals to the photocurrent. The generated photocurrent is proportional to the accumulated intensities of the WDM optical signals, which is the square of optical magnitudes. Thus the generated photocurrent at the right and left output PDs, I^0 and I^1 , can be expressed as,

$$\begin{aligned} \begin{pmatrix} I^0 \\ I^1 \end{pmatrix} &\propto \frac{1}{2} \begin{pmatrix} R^0 \sum_{i=0}^{N-1} \|x_i + y_i\|^2 \\ R^1 \sum_{i=0}^{N-1} \|j(x_i - y_i)\|^2 \end{pmatrix}, \\ &\propto \frac{1}{2} \begin{pmatrix} \sum_{i=0}^{N-1} R^0 (x_i + y_i)^2 \\ \sum_{i=0}^{N-1} R^1 (x_i - y_i)^2 \end{pmatrix}, \end{aligned} \quad (5)$$

where R_0 and R_1 are the responsivities of the photo-diodes on the right and left output ports of DC, respectively. Subtraction between the two currents is realized by the balanced photodetection, producing the output current as,

$$\begin{aligned} I_o &\propto R^0 \sum_{i=0}^{N-1} (x_i + y_i)^2 - R^1 \sum_{i=0}^{N-1} (x_i - y_i)^2 \\ &\propto R \left(\sum_{i=0}^{N-1} (x_i + y_i)^2 - \sum_{i=0}^{N-1} (x_i - y_i)^2 \right) \\ &\propto R \left(\sum_{i=0}^{N-1} x_i y_i \right) \propto \vec{x} \cdot \vec{y} \end{aligned} \quad (6)$$

$R_0 = R_1 = R$ for the balanced PD arrangement. The resultant output carries the dot-product result between \mathbf{x} and \mathbf{y} , which can be obtained by simply scaling the output current.

Our proposed DDot architecture leverages the WDM technique to enable vector dot-product using only one DC and one PS, achieving superior computing density. The PS and DC devices are entirely passive at the fixed configuration, resulting in zero energy consumption, no external control overhead, and no thermal crosstalk concern. One of the key advantages of DDot is that it allows both operands to be optically encoded at high speed without almost no additional mapping overhead, a crucial feature sought after to support dynamic MM in Transformers.

3.2 DPTC : Dynamically-Operated Photonic Tensor Core

To support matrix multiplication (MM), we can decouple MM into vector dot-products and map those dot-products onto our DDot engine. However, simply mapping each vec-

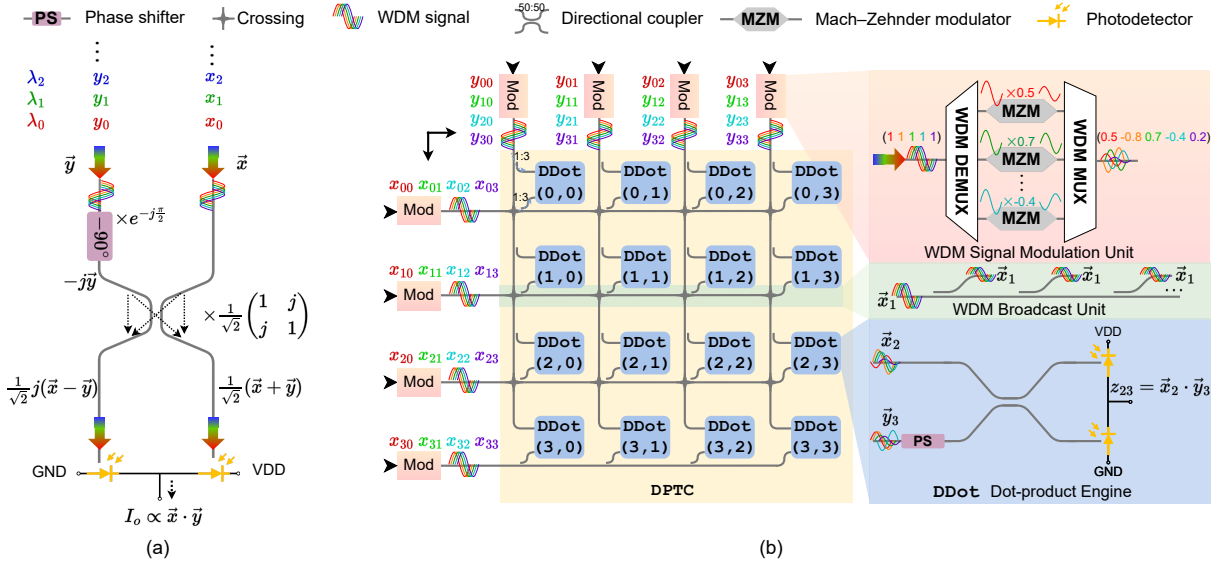


Figure 2: (a) The proposed DDot dot-product engine. Multi-wavelength signals propagate concurrently on the waveguide. (b) The proposed DPTC matrix-matrix multiplication unit with input WDM signals broadcasting.

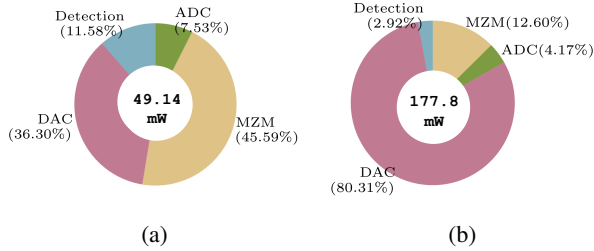


Figure 3: Power breakdown of (a) a 4bit DDot engine and (b) an 8bit DDot engine. Both implement a len-4 dot-product and work at 5 GHz. The key components in DDot is included (DAC [7], ADC [27], MZM [41], Photodetector [48] and the transimpedance amplifier (TIA) [38]). The power of DAC and ADC have been scaled according to the working frequency and bit-width following [23].

tor dot-product onto an individual DDot [1, 43] could lead to nontrivial signal modulation overhead and impede overall system efficiency when supporting MM. Consider a DDot engine implementing a dot-product between two length- k vectors, we require $2k$ Digital-to-Analog Converters (DAC) and $2k$ high-speed MZMs to achieve operand encoding. Hence, when k is large, the signal modulation part, including DAC and MZM, will dominate the overall power consumption. Figure 3 illustrates the power breakdown for two DDot engines implementing a length-4 vector dot-product with 4-bit and 8-bit precision. Despite the relatively small $k = 4$, the signal modulation constitutes 70-90% of the total power consumption. To support higher bit-width, such as 8-bit, DAC takes up to 80% of total power, as capacitive DAC consumes much more power in high-resolution settings [23]. Therefore, a more efficient design with optimized modulation cost is in high demand, enabling the utilization of DDot engines to construct MM units beyond vector dot-product units.

We introduce a novel photonic tensor core design called

DPTC, which leverages DDot dot-product engines to efficiently perform ultra-parallel matrix multiplication with highly reduced modulation overhead. Figure 2(b) illustrates the architecture of the proposed DPTC design. A DPTC engine has a shape of $N_v \times N_h$, where N_v and N_h represent the numbers of input bus waveguides along the vertical and horizontal directions, respectively. The optical inputs are driven by coherent sources with phase shifters to control their phases. Each waveguide in the DPTC features a WDM signal modulation unit where each element of length- N_λ vector is encoded at a unique wavelength using high-speed MZM. Within the modulation unit, a WDM demultiplexer (DEMUX) separates the multi-wavelength light sources into individual MZMs for signal encoding. The input's sign can be encoded to the phase of the light signals, i.e., -1 corresponds to a π phase shift, which is the fundamental mechanism to support the full-range representation of the input operands. Then, a WDM multiplexer (MUX) combines multiple wavelengths into a single light beam. The N_λ -wavelength input WDM signals propagate simultaneously along the waveguide. At each intersection node of the vertical and horizontal waveguides, two directional couplers are used to couple a fixed amount of light out of the two bus waveguides, feeding a copy of the input vectors to the DDot engine. The DDot engine accepts the two coupled optical signals as input and performs a dot-product calculation for two length- N_λ vectors. With $N_v \times N_h$ DDot units in the DPTC, where each performs a length- N_λ dot-product, DPTC is capable of calculating a $[N_h, N_\lambda] \times [N_\lambda, N_v]$ MM in one shot.

Consider DDot (i, j) at the intersection of the i -th horizontal waveguide and the j -th vertical waveguide. To ensure the correct light power distribution that each DDot unit receives the same fraction of input light for computation, we must account for the gradual reduction of light power along the waveguide caused by the previous coupling. Therefore, neglecting loss of the waveguide crossings, directional coupler, and propagation, the splitting ratios of couplers on the ver-

tical and horizontal waveguides, $\text{Ratio}_{(i,j)}^v$ and $\text{Ratio}_{(i,j)}^h$, are chosen to provide an equal power splitting as follows,

$$\text{Ratio}_{(i,j)}^v = \frac{1}{N_v - j}, \text{Ratio}_{(i,j)}^h = \frac{1}{N_h - i}. \quad (7)$$

We can further consider the signal loss to adjust the splitting ratio. This kind of crossbar-style photonic design based on directional couplers has been successfully demonstrated in [15]. Additionally, the light power between the vertical waveguide and horizontal waveguide should follow a ratio $N_h : N_v$. The selection of splitting ratios ensures no waste of light power, as the last coupler on the corresponding waveguide will use all the remaining light for computation. Moreover, incoming signals at input ports of DDot unit may have phase differences due to their optical path differences. The phase differences can be pre-calibrated during modulation with MZMs.

The proposed DPTC photonic tensor core design represents a significant advancement over prior ONNs with superior flexibility, as it is the first integrated photonic arithmetic unit capable of performing matrix multiplication between two *dynamically* encoded optical signals. In contrast to most previous designs that only supported MVM, our DPTC enables a one-shot implementation of MM with ultra-high computation parallelism. Moreover, leveraging the broadcast ability of light, we maximize the sharing of the modulated signals among multiple DDot units along the same waveguide to amortize the modulation overhead. Specifically, for the $[N_h, N_\lambda] \times [N_\lambda, N_v]$ matrix-matrix multiplication, the modulation energy cost E_{mod} of our DPTC can be computed as

$$E_{mod} \approx (N_h N_\lambda + N_\lambda N_v)(E_{DAC} + E_{MZM}). \quad (8)$$

On the other hand, if we map each dot-product into individual DDot using a similar architecture design [1, 43], the modulation cost would be

$$E_{mod} \approx (N_h N_v \cdot (2N_\lambda))(E_{DAC} + E_{MZM}), \quad (9)$$

where $N_h N_v$ is the number of dot-products in the MM, and each dot-product computation requires encoding two length- N_λ vectors. Hence, our DPTC achieves $\frac{2N_h N_v}{N_h + N_v}$ times less modulation cost, which is essential to preserve the energy efficiency superiority of our design over prior works.

3.3 Robustness Analysis of Photonic Design

Optical computing systems are subject to a variety of noises, such as optical encoding noise, WDM dispersion, and hardware imperfection. Here, we analyze the robustness of the proposed photonic tensor core DPTC design by deeply investigating its basic computation component DDot.

Optical Encoding Noise. In our dynamic-operated photonic tensor core, both operands are encoded in analog optical signals. As analog signals, it inevitably encounters encoding noise, including stochastic dynamic drift in both the magnitude and phase of the optical signal. Specifically, consider two operands x and y encoded in optical domain, we have $x' = (x + \delta x)e^{j\delta\phi_x}$ and $y' = (y + \delta y)e^{j\delta\phi_y}$, where δx and δy denote the magnitude drift, and $\delta\phi_x$ and $\delta\phi_y$ denote the phase drift. For simplicity, we extract the relative phase drift between the two operands and express it as an equivalent dynamic phase drift $\delta\phi_d$. Phase drift is estimated to follow a

Gaussian distribution $\mathcal{N}(0, \sigma_\phi^2)$, and the magnitude drift is dependent on which value v we want to encode, which is estimated using a Gaussian distribution with $\delta v = \mathcal{N}(0, (\sigma_v v)^2)$.

Considering the optical encoding noise, we have the transfer function of our DDot engine, i.e., Eq. (4), as,

$$\begin{aligned} \begin{pmatrix} z_i^0 \\ z_i^1 \end{pmatrix} &= \frac{1}{\sqrt{2}} \begin{pmatrix} 1 & j \\ j & 1 \end{pmatrix} \begin{pmatrix} 1 & 0 \\ 0 & e^{-j\pi/2} \end{pmatrix} \begin{pmatrix} \hat{x}_i \\ \hat{y}_i e^{j\delta\phi_{d_i}} \end{pmatrix} \\ &= \frac{1}{\sqrt{2}} \begin{pmatrix} 1 & j \\ j & 1 \end{pmatrix} \begin{pmatrix} 1 & 0 \\ 0 & e^{-j(\pi/2 - \delta\phi_{d_i})} \end{pmatrix} \begin{pmatrix} \hat{x}_i \\ \hat{y}_i \end{pmatrix}, \quad (10) \\ &= \frac{1}{\sqrt{2}} \begin{pmatrix} (\hat{x}_i - \sin\phi_i \hat{y}_i) + j\hat{y}_i \cos\phi_i \\ \hat{y}_i \cos\phi_i + j(\hat{x}_i + \sin\phi_i \hat{y}_i) \end{pmatrix} \end{aligned}$$

where $\phi_i = \delta\phi_{d_i} - \pi/2$, $\hat{x}_i = x + \delta x_i$ and $\hat{y}_i = y + \delta y_i$.

Hence, based on Eq. (6), we can obtain the output photocurrent under encoding noise as,

$$\begin{aligned} I_o &\propto R(P^0 - P^1) \propto \left(\sum_{i=0}^{N-1} \hat{x}_i \hat{y}_i \sin -\phi_i \right) \\ &\begin{pmatrix} P^0 \\ P^1 \end{pmatrix} \propto \frac{1}{2} \begin{pmatrix} \sum_{i=0}^{N-1} (\hat{x}_i - \sin\phi_i \hat{y}_i)^2 + (\hat{y}_i \cos\phi_i)^2 \\ \sum_{i=0}^{N-1} (\hat{y}_i \cos\phi_i)^2 + (\hat{x}_i + \sin\phi_i \hat{y}_i)^2 \end{pmatrix}. \quad (11) \end{aligned}$$

As shown above, each scalar product $x_i y_i$ has a non-ideal noise scaling factor $\sin\phi_i$ introduced by the phase shift. However, our engine is highly robust to this term since ϕ_i is a perturbed value around $-\pi/2$, which is the local optima of the sin function with the minimum sensitivity to perturbation.

WDM Dispersion. Our architecture leverages wavelength division multiplexing (WDM) to unleash the parallel computing capacity of photonics, allowing multiple wavelengths to work independently without interfering. Nevertheless, even with the adoption of broadband devices (coupler, phase shifter), photonic circuits still exhibit slightly different responses to different working wavelengths. Specifically, the wavelength-dependent transfer function of the directional coupler is described by

$$\begin{pmatrix} t & kj \\ kj & t \end{pmatrix}, \quad (12)$$

where $t = \sqrt{1 - \kappa(\lambda)}$ and $k = \sqrt{\kappa(\lambda)}$, the optical transmission and coupling coefficients. $\kappa(\lambda)$ is a wavelength-dependent power coupling coefficient of the coupler. It is computed as $\kappa(\lambda) = \sin^2((\pi L_c(\lambda_0))/4L_c(\lambda))$, where L_c is the wavelength-dependent 100% coupling length of the directional coupler. κ is designed to be 1/2 at the design(center) wavelength λ_0 . Moreover, the phase response of the phase shifter follows $\Delta\phi(\lambda) = 2\pi\Delta n_{\text{eff}}L/\lambda$, which is wavelength-dependent as well. In this paper, we choose the wavelength channel spacing as 0.4 nm based on DWDM and center wavelength $\lambda_0 = 1.55\text{nm}$. We sweep 25 wavelengths around the center wavelength and show the corresponding κ and ϕ in Figure 5. The maximum relative difference of κ between the center wavelength and the furthest wavelength would be $\sim 1.8\%$. The maximum dispersion-induced phase difference is 0.28° compared to the desired phase -90° .

To further understand the impact of DC's WDM dispersion on the computed output, we substitute the response of the directional coupler with the wavelength-dependent ones in Eq.(10). The wavelength-dependent transfer function of

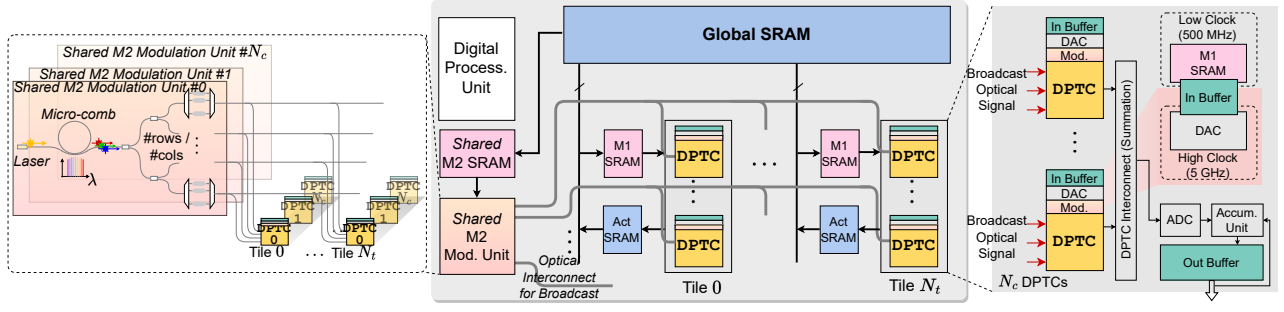


Figure 4: High-level architecture of the proposed DOTA. It has a three-level memory hierarchy, multiple photonic analog computing tiles/cores, on-chip multi-wavelength light source, and optical interconnect for data broadcast.

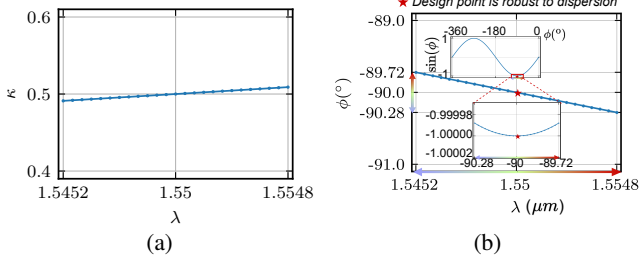


Figure 5: Our design point is robust to non-ideal dispersion effects. The coupling coefficient κ and the phase shift ϕ are not sensitive to the wavelength-dependent device responses (i.e., dispersion).

DDot can be obtained as

$$\begin{pmatrix} z_i^0 \\ z_i^1 \end{pmatrix} = \begin{pmatrix} (t_i \hat{x}_i - k_i \hat{y}_i \sin \phi_i) + j k_i \hat{y}_i \cos \phi_i \\ t_i \hat{y}_i \cos \phi_i + j (k_i \hat{x}_i + t_i \hat{y}_i \sin \phi_i) \end{pmatrix}. \quad (13)$$

Thus, the output photocurrent becomes

$$\begin{aligned} I_o &\propto \sum_{i=0}^{N-1} \left(\frac{(k_i^2 - t_i^2) \hat{x}_i^2 + (t_i^2 - k_i^2) \hat{y}_i^2}{2} + 2t_i k_i \hat{x}_i \hat{y}_i \sin -\phi_i \right) \\ &\propto \sum_{i=0}^{N-1} \left(\frac{(2k_i^2 - 1) \hat{x}_i^2 + (1 - 2k_i^2) \hat{y}_i^2}{2} + 2k_i \sqrt{1 - k_i^2} \hat{x}_i \hat{y}_i \sin -\phi_i \right) \end{aligned} \quad (14)$$

where an additive error relative to \hat{x}^2 and \hat{y}^2 is introduced.

Note that in our DDot engine, all encoded data are mapped into the MZM modulation range $[-1, 1]$. Hence, given a b -bit data, considering the full-range quantization without offset, the data is quantized into the range of $[-\alpha 2^{b-1}, \alpha(2^{b-1} - 1)]$, where α is the quantization scale. We need first to divide the data by the max absolute value $\alpha 2^{b-1}$ such that we can map the data on DDot. Hence, denote the two unscaled operands of the dot-product to be $\tilde{\mathbf{x}}$ and $\tilde{\mathbf{y}}$, the input of DDot is $\mathbf{x} = \tilde{\mathbf{x}}/\beta_x$ and $\mathbf{y} = \tilde{\mathbf{y}}/\beta_y$, where $\beta_x = 2^{b-1} * \alpha_x$ and $\beta_y = 2^{b-1} * \alpha_y$. Based on Eq. (13), we have the $\tilde{\mathbf{x}} * \tilde{\mathbf{y}}$ as,

$$\begin{aligned} \tilde{\mathbf{x}} * \tilde{\mathbf{y}} &= \beta_x \beta_y \text{DDot}(\tilde{\mathbf{x}}/\beta_x, \tilde{\mathbf{y}}/\beta_y) = \beta_x \beta_y \text{DDot}(\mathbf{x}, \mathbf{y}) \\ &= \beta_x \beta_y \sum_{i=0}^{N-1} \left(\frac{p_i (\frac{\hat{x}_i}{\beta_x})^2 - p_i (\frac{\hat{y}_i}{\beta_y})^2}{2} + 2t_i k_i \frac{\hat{x}_i}{\beta_x} \frac{\hat{y}_i}{\beta_y} \sin -\phi_i \right), \quad (15) \\ &= \sum_{i=0}^{N-1} 2k_i \sqrt{1 - k_i^2} \hat{x}_i \hat{y}_i \sin -\phi_i + \sum_{i=0}^{N-1} \frac{p_i}{2} \left(\frac{\beta_y \hat{x}_i^2}{\beta_x} - \frac{\beta_x \hat{y}_i^2}{\beta_y} \right) \end{aligned}$$

where $p_i = 2k_i^2 - 1$. As shown above, the two additive error

terms \hat{x}_i^2 and \hat{y}_i^2 will be naturally scaled to be in the similar range such that they can be compensated during computation.

The term $2k_i \sqrt{1 - k_i^2}$ and $\sin \phi_i$ are very robust to the perturbation induced by WDM dispersion, as our design points $k = \frac{1}{\sqrt{2}}$ and $\phi = -\frac{\pi}{2}$ are the local optimal of $x\sqrt{1 - x^2}$ and \sin with minimum sensitivity to perturbation.

Other Errors To further simulate the other errors, such as photo-detection error, device imperfection, and imperfect coupling ratios of direction couplers, we add Gaussian noise to the final computation outputs when simulation of Transformer running on our DDot-based DPTC. In this paper, we add a multiplicative noise to each output, $\mathcal{N}(1, 0.05^2)$.

4. PROPOSED DOTA ACCELERATOR

In this section, we present the high-level architectural design of the proposed DOTA accelerator.

4.1 Overall System Design

The DOTA architecture is designed for Transformer that contains analog photonic computing units for General matrix multiplication (GEMM) operations, and underlying electronics for other operations, including signal conversion, data storage, nonlinearity functions, and SoftMax.

Architecture Overview. Figure 4 illustrates the overall micro-architecture of the proposed micro-architecture with a particular emphasis on the photonic computing part. DOTA incorporates multiple photonic tensor cores (DPTC) into a single chip to increase the amount of parallel processing. We cluster N_c DPTC into one tile, and we have N_t tiles in total in the DOTA accelerator. All the photonic tensor cores are clocked at 5GHz for a conservative assumption. Note that the photonic part can run faster, such as 10GHz [25]. The operands of each DPTC undergo an electrical-to-optical conversion (E/O) with digital-to-analog converters (DAC), and the outputs of DPTC need analog-to-digital converts (ADC) to bring the analog result back to the digital domain. We have digital processing units to process non-GEMM operations needed in Transformer.

For the memory part, we have a large 2MB global SRAM, which interacts with DRAM and is responsible for holding inputs, activations, and weights. The size of the global SRAM is designed to be sufficient for storing activations for most Transformers. In addition, each tile has its own 4KB SRAM to hold the operands for the matrix multiplication that the tile is performing, as well as an activation SRAM to store the computed results. Since the photonic part of our accelerator

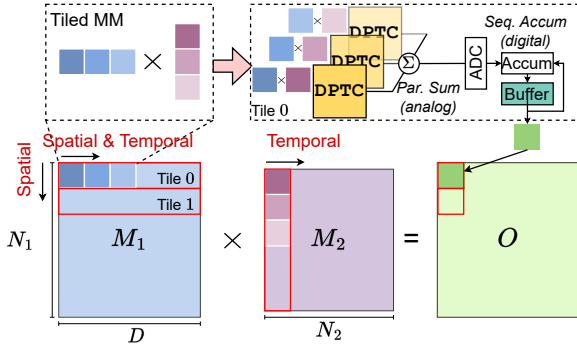


Figure 6: Illustration of the tiling and spatial/temporal mapping for processing GEMM.

Table 2: Table of notations used in the accelerator design

Notation	Definition
N_h	# input horizontal waveguides of each DPTC
N_v	# input vertical waveguides of each DPTC
N_λ	# wavelengths of each DPTC
N_c	# photonic tensor cores in each tile
N_t	# tiles in our accelerator

runs at a clock speed of 5GHz, and our DPTC unit handles one small matrix multiplication in one clock cycle, the required data bandwidth is high. To address this, we follow [9] and decouple the large SRAM array into smaller 32KB sub-arrays. This improves data bandwidth by reading data from these sub-arrays with a small shifting interval. Data buffers are used for each photonic tensor core DOTA to communicate the DACs and SRAM in different clock domains.

DOTA uses OS dataflow and explores the superiority of optical interconnect to enable data broadcast to efficiently support GEMM operations, which will be elaborated on later. **Photonic Tensor Cores.** Photonic tensor core DPTC works with its necessary digital components, including DACs, ADCs, TIAs, and data buffers. The photonic computing part is clocked at 5 GHz and operates at 4-bit precision by default. Our DPTC is capable of implementing $[N_h, N_\lambda] \times [N_\lambda, N_v]$ matrix-matrix multiplication in one cycle. Large GEMM operations in Transformer are mapped onto on-chip DPTC by using tiled matrix-matrix multiplication.

Digital Processing Units. We assume all other non-GEMM operations are implemented using digital electronics.

4.2 Dataflow

Our DPTC frees the selection of dataflow by having both operands dynamically encoded at high-speed. Most prior ONNs typically map one operand into photonic circuit states that are slow to reconfigure or that need operand decomposition at run-time. This kind of design concept limits its dataflow selection, making them only suitable for weight-stationary (WS) dataflow [9]. Note that the WS stationary dataflow in ONNs is not the same as that of the digital electronics accelerator design. They indeed have one operand (usually the weight) being statically encoded in the photonic circuit, while the normal WS stationary dataflow is a design principle to explore data locality and improve data reuse.

In DOTA, we adopt a unified output-stationary (OS) dataflow to accelerate all the GEMM operations in the Transformer.

The OS dataflow enables us to minimize the on-chip buffer requirements [28, 52] and allows us to adopt customized optimization techniques to reduce the cross-domain signal conversion overhead in our mixed-signal accelerator, i.e., A/D/D-A conversion. To support GEMM on our DOTA with multiple DPTC, we consider fine-grained tiling and carefully design the spatial/temporal mappings. As illustrated in Figure 6, we use the OS dataflow as the basic design principle for calculating matrix multiplication between M_1 and M_2 . Specifically, we tile matrix M_1 along the N_1 dimension and map them to different tiles spatially. Each tile is responsible for calculating the multiplication result between one tiled row of M_1 and matrix M_2 temporally. At each cycle, each tile handles tiled matrix multiplication. Since we have multiple DPTC in each spatial unit, we distribute the tiled MM workload among these cores. The outputs of multiple cores are first accumulated by photocurrent summation in the analog domain, followed by A/D conversion. Then the partial sums are sent to the output buffer for further sequential accumulation in the digital domain. This analog domain partial summation can not only reduce the required A/D conversion cost but also avoid the precision loss during A/D conversion with full-precision photocurrent summation.

4.3 Architecture-Level Optimization

The expensive operand encoding and cross-domain signal conversion remain to be the key bottleneck for emerging photonic systems, which is also true in our system. Therefore, we consider the two following optimization opportunities to reduce the modulation and signal conversion cost.

4.3.1 Operand Broadcast via Optical Interconnect

As shown in Figure 6, different tiles process the multiplication between different chunks of M_1 and the same chunk of M_2 . This allows sharing the M_2 part across different tiles. In this scheme, the DACs and MZMs used to encode operands can be shared among tiles using global modulation units as shown in Figure 4, leading to N_t times energy saving. Thanks to the superiority of optics in signal broadcast, these modulated signals are efficiently broadcast to each DPTC that shares the same operand via optical interconnect.

4.3.2 Analog-Domain Temporal Accumulation with Time Integral

Since our DPTC design supports efficient dynamic operand switching, we adopt the OS dataflow that can potentially enable analog-domain temporal accumulation [25, 54] via time integral to reduce the ADC overhead. This technique is not applicable to prior WS accelerators since their output results are accumulated to different buffer locations across time steps, preventing the utilization of analog temporal accumulation. Analog temporal accumulation involves accumulating results using photodetectors and capacitors to store charges, which can be read at a later time. This allows the ADC to operate at a lower frequency, significantly reducing power consumption. Additionally, by performing accumulation before signal digitization in ADCs, full-precision partial summation is achieved in the analog domain, leading to improved accuracy [25]. In this paper, we set the analog temporal accumulation depth to 3, i.e., A/D conversion happens once every three analog accumulation steps.

Table 3: Adopted component parameters in DOTA. IL represents insertion loss, and FSR means free spectral range.

Device	Parameter	Value
DAC [7]	Precision	8-bit
	Power	50 mW (@14GSPS)
	Area	11,000 μm^2
ADC [27]	Precision	8-bit
	Power	14.8 mW (@10GSPS)
	Area	2,850 μm^2
TIA [38]	Power area	3 mW <50 μm^2
Microdisk [45]	Locking Power	0.275 mW ¹
	IL	0.93 dB
	Area	4.8 \times 4.8 μm^2
	FSR	5.6 THz (55.1 nm)
Microring Resonator	Tuning Power	0.21 mW
	Locking Power	1.2 mW/0.5FSR [41]
	IL	0.95 dB [33]
MZM	Area	9.66 \times 9.66 μm^2 [33]
	Tuning Power	2.25 mW [12]
	IL	1.2 dB [2]
Directional Coupler [51]	Area	260 \times 20 μm^2 [2]
	IL	0.33 dB
MEMS Phase Shifter [35]	Area	5.25 \times 2.4 μm^2
	IL	0.33 dB
Photodetector [21]	Response Time	100 \times 45 μm^2
	Power	2 μs
	Sensitivity	1.1mW -25 dBm
Y-branch [30]	Area	4 \times 10 μm^2
	IL	0.3 dB
Frequency Micro-comb	Area	1.8 \times 1.3 μm^2
On-chip Laser	Wall-plug Efficiency	0.2
	Area	400 \times 300 μm^2

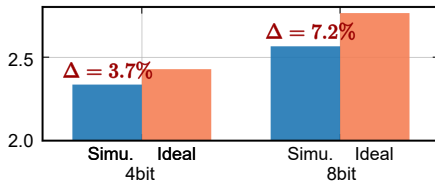


Figure 7: Optical simulation results of 4-bit and 8-bit random length-12 dot-products on our DDOT engine.

5. EVALUATION

5.1 Experiment Setup

System Setup. We build a Python-based simulator to simulate the latency, power, area, and efficiency of DOTA on actual Transformer inference. The area, leakage power, and access energy of the memory system are modeled using PRACTI [39] in 14 nm. We use high-bandwidth memory (HBM) to supply data to the photonic system with a memory system bandwidth $>1\text{TB/s}$ [31]. The power and energy cost of digital processing units is obtained from [19, 34, 50]. We use the ADC [27] and DAC [7] with similar technology nodes (14 nm and 16 nm), while their bit-widths and frequency do not precisely match our settings. We follow [23] to scale the ADC and DAC power according to the bit-width and frequency requirement of the photonic computing units. Table 3 lists the parameters for used photonic devices. The laser power is set to meet the minimum power requirement of the photodetector considering system loss and is scaled based on the precision requirement [43]. During simulation, the

Table 4: Base (B) and Large (L) configurations for DOTA.

Ours	N_t	N_c	N_h	N_v	N_λ	Global SRAM (MB)	area (mm^2)
DOTA-B	4	2	12	12	12	2	60.33
DOTA-L	8	2	12	12	12	4	112.88

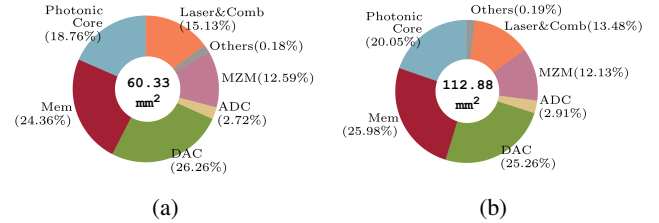


Figure 8: Area breakdown of our (a) DOTA-B and (b) DOTA-L by component.

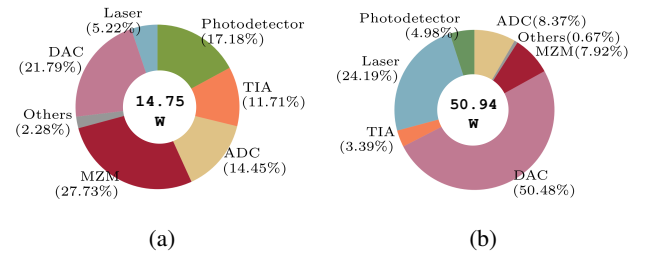


Figure 9: Power breakdown of our DOTA-B for two precision settings. (a) 4-bit, (b) 8-bit.

simulator implements the detail of the tiling algorithm and uses a batch size of 1. The deep pipeline of the photonic/digital processing unit is not adopted in this paper, which can be employed to further improve the system performance [9].

Functionality Validation. We use Lumerical INTERCONNECT tools [29] with the AMF process design kit (PDK) to validate the functionality of our DDOT engine. 12 wavelengths are used, and the dot-product error on two random length-12 dot-product is 3.7 – 7.2%, as shown in Figure 7.

Models, Datasets, and Training Settings. We use DeiT [46] and BERT [10] to evaluate the efficiency and accuracy. Both are well-recognized Vision and NLP Transformers. We apply low-bit quantization on both weight and activation [14]. Noise-aware training is adopted by injecting optical encoding noise and output detection noise. We inject all variations discussed in Section 3.3 to test the accuracy during inference. **DOTA Architecture Configurations.** In this paper, we design two sets of accelerators called DOTA-B and DOTA-L. Table 4 lists their detailed parameters. DOTA-L doubles the number of tiles to increase its throughput for large models.

5.2 System Efficiency Analysis

Area Breakdown. Figure 8 illustrates the area breakdown of our DOTA-B and DOTA-L architecture. The DOTA-B has 60.33 mm^2 which is around half of the area of the DOTA-L architecture (112.88 mm^2). For each architecture, the photonic core, memory, and DAC contribute the largest portion of the area, with around 20%, 25%, and 25% share, respectively. The remaining components, such as laser, ADC, and MZM, account for less than 25% of the overall area.

Power Breakdown. Figure 9 shows the power consumption

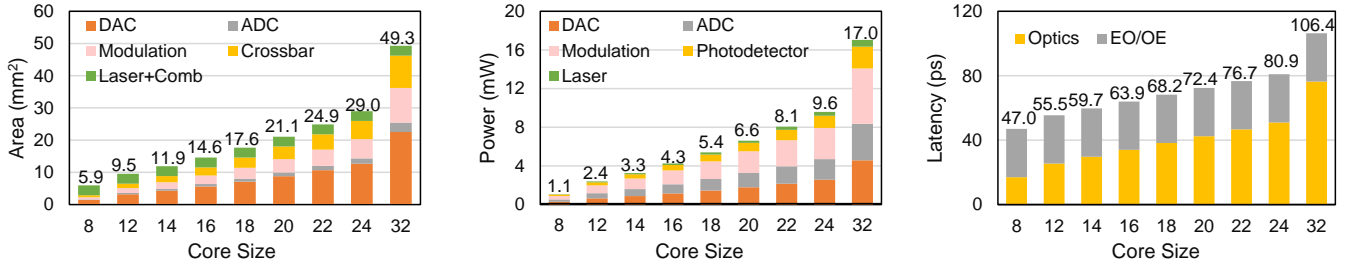


Figure 10: Area, power, and latency scaling evaluation with larger DPTC core sizes.

Table 5: Comparison to prior photonic accelerators. The MZI-based accelerator cannot support dynamic matrix multiplication in MHA operations. We assume MRR arrays implement its MHA. Previous designs have suffered from (1) one operand being statically encoded without the ability to be frequently updated, (2) limitations on operand range, or (3) high modulation costs.

Precision	Model	Module	MZI-based Accelerator [40]			MRR-based Accelerator [44]			DOTA-B		
			Energy↓ (mJ)	Latency↓ (ms)	EDP↓ (mJ*ms)	Energy↓ (mJ)	Latency↓ (ms)	EDP↓ (mJ*ms)	Energy↓ (mJ)	Latency↓ (ms)	EDP↓ (mJ*ms)
4-bit	DeiT-T	MHA	-	-	-	0.20	0.02	0.003	0.04	1.56e-3	7.00e-5
		FC	1.88	6.27	11.80	1.12	0.11	0.120	0.23	1.04e-2	2.45e-3
	DeiT-B	MHA	-	-	-	0.98	0.06	0.063	0.17	6.24e-3	1.06e-3
		FC	30.13	100.24	3020.20	17.88	1.72	30.784	3.75	1.67e-1	6.26e-1
Average Ratio			7.69	550.90	4237.25	4.76	10.29	48.998	1	1	1
8-bit	DeiT-T	MHA	-	-	-	0.51	0.02	0.008	0.15	1.56e-3	2.39e-4
		FC	19.77	6.27	123.87	2.18	0.11	0.235	0.68	1.04e-2	7.09e-3
	DeiT-B	MHA	-	-	-	3.91	0.06	0.251	0.60	6.24e-3	3.77e-3
		FC	158.18	50.12	7927.84	17.46	0.86	15.031	5.43	8.36e-2	4.54e-1
Average Ratio			26.14	550.90	14403.23	3.31	10.30	34.093	1	1	1

breakdown for DOTA-B for two data precision settings, 4-bit and 8-bit. The DOTA-L has a similar power breakdown with 28.06 W for 4-bit and 95.92 W for 8-bit. In our DOTA design, all operands are dynamically encoded, resulting in the operand encoding part, which includes the DAC and MZM, consuming the majority of the power. The reported operand modulation cost has been optimized through operand sharing at both the core and system levels. The 8-bit DOTA-B architecture consumes more than three times the power of the 4-bit architecture. This increase is primarily attributed to the higher power consumption of the high-bit DACs, which account for over 50% of the overall power in the 8-bit architecture. Additionally, the power consumption of the laser also significantly increases from 0.77 W to 12.3 W in order to achieve higher output precision.

Area, Power, Latency and Performance Scaling. In Figure 10, we show how the area, power consumption, and latency scale with the size of DPTC. The area increases from 5.9 mm² to 49.3 mm² when we increase the core size from 8 to 32. The ratio of each part roughly remains the same. For power consumption, it increases from 1.1 mW to 17 mW as the core size increases from 8 to 32, and the modulation, ADC, and DAC take the lion's share of the overall power consumption. Interestingly, the latency scaling shows a different pattern from the area and power consumption. The EO/OE latency remains almost the same regardless of the core size, while the optics latency increases approximately linearly with the size. As shown in Figure 11, we further show the performance and efficiency scaling of our design. As the core size increases, the performance (TOPS), area efficiency (TOPS/mm²), and energy efficiency (TOPS/W) increase while the energy efficiency per unit area (TOPS/W/mm²) decreases due to the

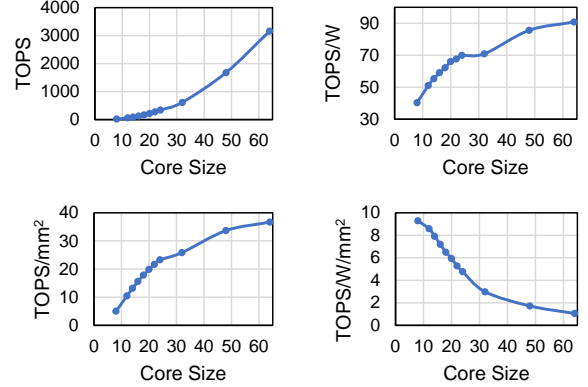


Figure 11: Performance and efficiency of the optical computing part (ADC/DAC excluded) scale with larger core size.

bottleneck of ADCs and DACs.

Wavelength Scaling. Thanks to the robust design points of our DPTC to non-ideal dispersion effects, we can increase the number of wavelengths to further boost the processing parallelism. In our system, we use Microdisk [45] as the filter to implement the WDM multiplexer and WDM demultiplexer. However, the microdisk imposes a free spectral range (FSR), which limits the system parallelism. Given its FSR=5.6 THz as shown in Table 3 and its design wavelength at 1550 nm, we can have its wavelength range as

$$\lambda_l = \frac{c}{f_0 + FSR/2} = 1527.88 \text{ nm}$$

$$\lambda_r = \frac{c}{f_0 - FSR/2} = 1572.76 \text{ nm} \quad (16)$$

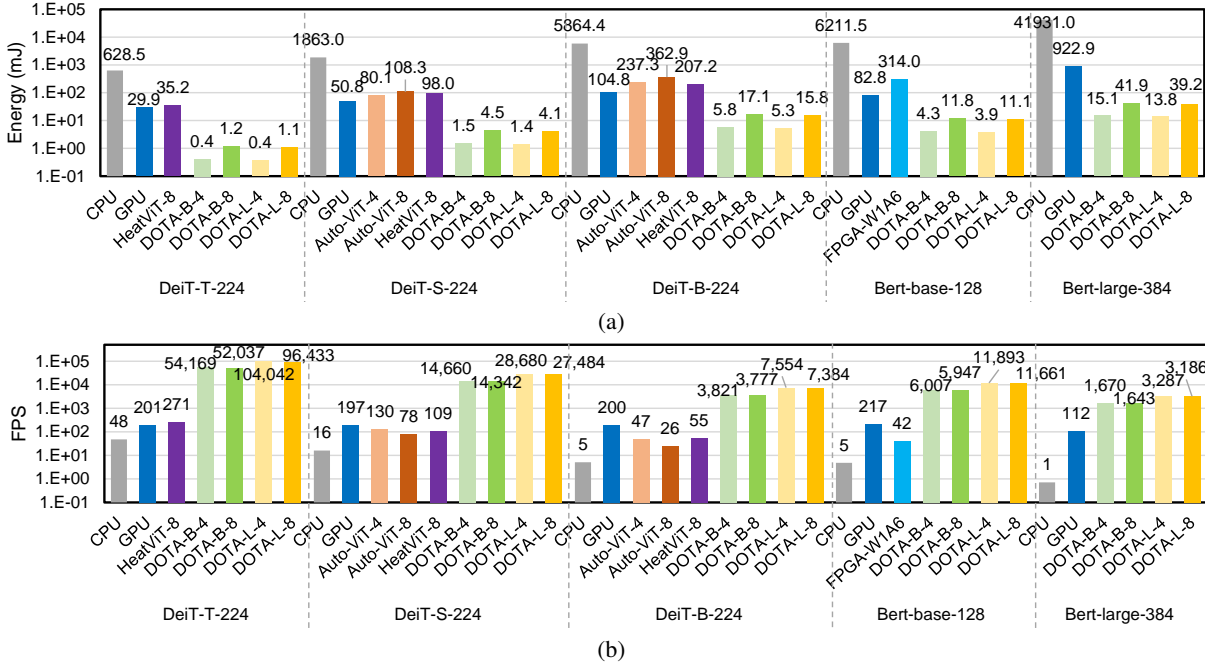


Figure 12: Compare (a) energy consumption (mJ) and (b) frames-per-second (FPS) across different accelerator designs on various workloads (DeiT-series with ImageNet1K-224x224 and BERT-series with 128 and 384 sequence lengths) and two different bitwidth (4-bit and 8-bit).

With channel spacing $\Delta\lambda = 0.4 \text{ nm}$, we can have a maximum of 112 wavelengths.

5.3 Compare to State-of-the-art Accelerators

How does DOTA compare to prior ONNs?

Since there are currently no available photonic accelerators specifically designed for Transformers, we have built a baseline system based on MRR weight banks [44]. To ensure a fair comparison, we scale the number of tensor cores in the MRR baseline to match the area of our DOTA design. Table 5 provides a detailed comparison between our proposed DOTA and previous ONNs. The results demonstrate the superior performance of DOTA in terms of energy consumption, latency, and energy-delay product (EDP). Specifically, under the 4-bit data representation, DOTA achieves energy, latency, and EDP reductions of $7.69\times$, $550.90\times$, and over $4,000\times$ compared to the MZI-based accelerator. Although the MRR-based architecture is more efficient than MZI, DOTA still outperforms it with energy, latency, and EDP reductions of $4.76\times$, $10.29\times$, and $49.00\times$, respectively. This superiority can be largely attributed to the limitations of MZI-based and MRR-based accelerators, which are constrained to performing only MVMs. Consequently, a greater number of cycles are required to complete matrix multiplication (MM) workloads, leading to increased energy consumption. Additionally, the MZI-based design suffers from high latency due to weight reprogramming, while the MRR-based design supports only positive input operands, resulting in doubled costs for full-range input support.

These comparisons highlight the superior performance and efficiency of our DOTA accelerator over prior ONNs in enabling the acceleration of Transformers workloads.

How does DOTA compare to SOTA digital electronics?

In Figure 12, we show the comparison results with several different hardware platforms. Specifically, we make comparisons with (1) one Nvidia A100 GPU, (2) Intel Core i7-9750H CPU, and (3) FPGA accelerators AutoViT [26] and HEATViT [11]. For GPU and CPU, we use automatic mixed precision to run the inference. For the FPGA, we use the results in the original paper. The results show that our DOTA consistently achieves the lowest energy consumption, with around $500\times$, $50\times$, and $20\times$ power reduction compared to CPU, GPU, and other domain-specific accelerators for Transformer. For throughput, DOTA also achieves the highest among all the platforms and gets 2 to 3 orders of magnitude higher FPS for various benchmarks.

5.4 Robustness Analysis

Furthermore, we evaluate the robustness of our design against random multiplicative input noises, additive phase noises, and dispersion effects. Figure 13 shows that on both workloads, our design is very robust to dispersion effects even with more than 20 wavelengths, showing less than 0.5% accuracy drop. The reason is that our design point of the directional coupler and phase shifters is the local minimum of their transmission, and also our specialized wavelength mapping method helps largely cancel the dispersion effects.

Figure 14 shows that our design demonstrates high tolerance to random input noises and device variations. On the DeiT-Tiny ImagenetNet workload, the noise-induced accuracy degradation is within 0.5% with a small variance.

6. CONCLUSION

The proliferation and increasing complexity of attention-based Transformers have spurred the need for efficient hardware accelerators. While electronic accelerators are widely

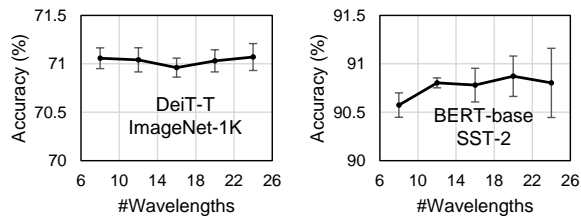


Figure 13: Dispersion robustness evaluation with a different number of wavelengths on DeiT-Tiny ImageNet1K and BERT-base SST2 workloads.

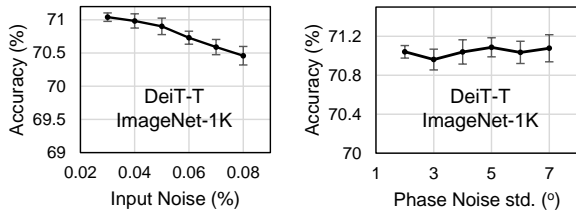


Figure 14: Input variation and phase noise robustness evaluation with different noise intensity on DeiT-Tiny ImageNet1K.

used, photonics has emerged as a compelling alternative due to its high energy efficiency and ultra-fast processing capabilities. Optical neural networks (ONNs) have shown promising results for convolutional neural network (CNN) workloads, which require only weight-static linear operations. However, the current SoTA photonic accelerators face challenges in efficiently supporting Transformer architectures with self-attention operations, primarily due to their inability to handle dynamic tensor multiplication and encode full-range operands. In this work, we introduce a customized, high-performance, and energy-efficient photonic Transformer accelerator, DOTA. We propose a novel photonic tensor core, a crossbar array of dynamic optical-optical vector dot-product engines. This design overcomes the fundamental constraints of existing ONNs, enabling highly parallel matrix multiplication with two dynamic, full-range input matrices. Our comprehensive evaluation shows that DOTA achieves over $4\times$ energy reduction and over $10\times$ latency reduction compared to prior photonic accelerators. Furthermore, it outperforms electronic Transformer accelerators with over $20\times$ energy reduction and 2 to 3 orders of magnitude lower latency.

Our work highlights the potential of photonics as a compelling alternative for efficient hardware accelerators tailored to advanced machine learning tasks. In the future, we anticipate significant advancements in photonic computing technologies, enhancing their flexibility, applicability, and performance across a broader range of machine learning tasks. Ongoing research in innovative cross-layer co-design will push the boundaries of what photonic accelerators can achieve and result in the creation of highly efficient, low-latency next-generation electronic-photonic computing systems capable of supporting increasingly complex ML workloads.

REFERENCES

- [1] S. Afifi, F. Sunny, M. Nikdast, and S. Pasricha, "Tron: Transformer neural network acceleration with non-coherent silicon photonics," *arXiv preprint arXiv:2303.12914*, 2023.
- [2] S. Akiyama, T. Baba, M. Imai, T. Akagawa, M. Takahashi, N. Hirayama, H. Takahashi, Y. Noguchi, H. Okayama, T. Horikawa *et al.*, "12.5-gb/s operation with $0.29\text{-}\mu\text{m}$ π I using silicon mach-zehnder modulator based on forward-biased pin diode," *Optics express*, vol. 20, no. 3, pp. 2911–2923, 2012.
- [3] M. G. Anderson, S.-Y. Ma, T. Wang, L. G. Wright, and P. L. McMahon, "Optical transformers," *arXiv preprint arXiv:2302.10360*, 2023.
- [4] J. L. Ba, J. R. Kiros, and G. E. Hinton, "Layer normalization," *arXiv preprint arXiv:1607.06450*, 2016.
- [5] T. Brown, B. Mann, N. Ryder, M. Subbiah, J. D. Kaplan, P. Dhariwal, A. Neelakantan, P. Shyam, G. Sastry, A. Askell *et al.*, "Language models are few-shot learners," *Advances in neural information processing systems*, vol. 33, pp. 1877–1901, 2020.
- [6] —, "Language models are few-shot learners," *Advances in neural information processing systems*, vol. 33, pp. 1877–1901, 2020.
- [7] P. Caragiulo, O. E. Mattia, A. Arbabian, and B. Murmann, "A compact 14 gs/s 8-bit switched-capacitor dac in 16 nm finfet cmos," in *2020 IEEE Symposium on VLSI Circuits*. IEEE, 2020, pp. 1–2.
- [8] N. Carion, F. Massa, G. Synnaeve, N. Usunier, A. Kirillov, and S. Zagoruyko, "End-to-end object detection with transformers," in *Computer Vision—ECCV 2020: 16th European Conference, Glasgow, UK, August 23–28, 2020, Proceedings, Part I 16*. Springer, 2020, pp. 213–229.
- [9] C. Demirkiran, F. Eris, G. Wang, J. Elmhurst, N. Moore, N. C. Harris, A. Basumallik, V. J. Reddi, A. Joshi, and D. Bunandar, "An electro-photonic system for accelerating deep neural networks," *arXiv preprint arXiv:2109.01126*, 2021.
- [10] J. Devlin, M.-W. Chang, K. Lee, and K. Toutanova, "Bert: Pre-training of deep bidirectional transformers for language understanding," *arXiv preprint arXiv:1810.04805*, 2018.
- [11] P. Dong, M. Sun, A. Lu, Y. Xie, K. Liu, Z. Kong, X. Meng, Z. Li, X. Lin, Z. Fang *et al.*, "Heatvit: Hardware-efficient adaptive token pruning for vision transformers," in *2023 IEEE International Symposium on High-Performance Computer Architecture (HPCA)*. IEEE, 2023, pp. 442–455.
- [12] P. Dong, W. Qian, H. Liang, R. Shafiiha, D. Feng, G. Li, J. E. Cunningham, A. V. Krishnamoorthy, and M. Asghari, "Thermally tunable silicon racetrack resonators with ultralow tuning power," *Optics express*, vol. 18, no. 19, pp. 20 298–20 304, 2010.
- [13] A. Dosovitskiy, L. Beyer, A. Kolesnikov, D. Weissenborn, X. Zhai, T. Unterthiner, M. Dehghani, M. Minderer, G. Heigold, S. Gelly, J. Uszkoreit, and N. Houlsby, "An image is worth 16x16 words: Transformers for image recognition at scale," in *International Conference on Learning Representations*, 2021. [Online]. Available: <https://openreview.net/forum?id=YicbFdNTTy>
- [14] S. K. Esser, J. L. McKinstry, D. Bablani, R. Appuswamy, and D. S. Modha, "Learned step size quantization," in *International Conference on Learning Representations*, 2020.
- [15] J. Feldmann, N. Youngblood, M. Karpov, H. Gehring, X. Li, M. Stappers, M. Le Gallo, X. Fu, A. Lukashchuk, A. S. Raja *et al.*, "Parallel convolution processing using an integrated photonic tensor core," *Nature*, 2021.
- [16] C. Feng, J. Gu, H. Zhu, Z. Ying, Z. Zhao, D. Z. Pan, and R. T. Chen, "A compact butterfly-style silicon photonic–electronic neural chip for hardware-efficient deep learning," *ACS Photonics*, vol. 9, no. 12, pp. 3906–3916, 2022.
- [17] J. Gu, Z. Zhao, C. Feng *et al.*, "Towards area-efficient optical neural networks: an FFT-based architecture," in *Proc. ASPDAC*, 2020.
- [18] J. Gu, Z. Zhao, C. Feng, Z. Ying, R. T. Chen, and D. Z. Pan, "O2NN: Optical Neural Networks with Differential Detection-Enabled Optical Operands," in *Proc. DATE*, 2021.
- [19] H. Guo, L. Peng, J. Zhang, Q. Chen, and T. D. LeCompte, "Att: A fault-tolerant rram accelerator for attention-based neural networks," in *2020 IEEE 38th International Conference on Computer Design*

- (ICCD). IEEE, 2020, pp. 213–221.
- [20] D. Hendrycks and K. Gimpel, “Gaussian error linear units (gelus),” *arXiv preprint arXiv:1606.08415*, 2016.
- [21] Z. Huang, C. Li, D. Liang, K. Yu, C. Santori, M. Fiorentino, W. Sorin, S. Palermo, and R. G. Beausoleil, “25 gbps low-voltage waveguide si-ge avalanche photodiode,” *Optica*, vol. 3, no. 8, pp. 793–798, 2016.
- [22] J. D. M.-W. C. Kenton and L. K. Toutanova, “Bert: Pre-training of deep bidirectional transformers for language understanding,” in *Proceedings of NAACL-HLT*, 2019, pp. 4171–4186.
- [23] Y. Kim, H. Kim, D. Ahn, and J.-J. Kim, “Input-splitting of large neural networks for power-efficient accelerator with resistive crossbar memory array,” in *Proceedings of the International Symposium on Low Power Electronics and Design*, 2018, pp. 1–6.
- [24] F. Koyama and K. Iga, “Frequency chirping in external modulators,” *Journal of Lightwave Technology*, vol. 6, no. 1, pp. 87–93, 1988.
- [25] S. Li, H. Yang, C. W. Wong, V. J. Sorger, and P. Gupta, “Photofourier: A photonic joint transform correlator-based neural network accelerator,” in *2023 IEEE International Symposium on High-Performance Computer Architecture (HPCA)*. IEEE, 2023, pp. 15–28.
- [26] Z. Lit, M. Sun, A. Lu, H. Ma, G. Yuan, Y. Xie, H. Tang, Y. Li, M. Leiser, Z. Wang *et al.*, “Auto-vit-acc: An fpga-aware automatic acceleration framework for vision transformer with mixed-scheme quantization,” in *2022 32nd International Conference on Field-Programmable Logic and Applications (FPL)*. IEEE, 2022, pp. 109–116.
- [27] J. Liu, M. Hassanpourghadi, and M. S.-W. Chen, “A 10gs/s 8b 25fj/c 2850um 2 two-step time-domain adc using delay-tracking pipelined-sar tdc with 500fs time step in 14nm cmos technology,” in *2022 IEEE International Solid-State Circuits Conference (ISSCC)*, vol. 65. IEEE, 2022, pp. 160–162.
- [28] L. Lu, Y. Jin, H. Bi, Z. Luo, P. Li, T. Wang, and Y. Liang, “Sanger: A co-design framework for enabling sparse attention using reconfigurable architecture,” in *MICRO-54: 54th Annual IEEE/ACM International Symposium on Microarchitecture*, 2021, pp. 977–991.
- [29] I. Lumerical Solutions, “Lumerical interconnect,” <https://www.lumerical.com/products/interconnect>, 2003.
- [30] D. P. Nair and M. Ménard, “A compact low-loss broadband polarization independent silicon 50/50 splitter,” *IEEE Photonics Journal*, vol. 13, no. 4, pp. 1–7, 2021.
- [31] M. O’Connor, N. Chatterjee, D. Lee, J. Wilson, A. Agrawal, S. W. Keckler, and W. J. Dally, “Fine-grained dram: Energy-efficient dram for extreme bandwidth systems,” in *Proceedings of the 50th Annual IEEE/ACM International Symposium on Microarchitecture*, 2017, pp. 41–54.
- [32] OpenAI, “Gpt-4 technical report,” 2023.
- [33] P. Pintus, M. Hofbauer, C. L. Manganelli, M. Fournier, S. Gundavarapu, O. Lemonnier, F. Gambini, L. Adelmini, C. Meinhardt, C. Kopp *et al.*, “Pwm-driven thermally tunable silicon microring resonators: design, fabrication, and characterization,” *Laser & Photonics Reviews*, vol. 13, no. 9, p. 1800275, 2019.
- [34] H. Prashanth and M. Rao, “Somalib: Library of exact and approximate activation functions for hardware-efficient neural network accelerators,” in *2022 IEEE 40th International Conference on Computer Design (ICCD)*. IEEE, 2022, pp. 746–753.
- [35] N. Quack, A. Y. Takabayashi, H. Sattari, P. Edinger, G. Jo, S. J. Bleiker, C. Errando-Herranz, K. B. Gylfason, F. Niklaus, U. Khan *et al.*, “Integrated silicon photonic mems,” *Microsystems & Nanoengineering*, vol. 9, no. 1, p. 27, 2023.
- [36] A. Radford, K. Narasimhan, T. Salimans, I. Sutskever *et al.*, “Improving language understanding by generative pre-training,” 2018.
- [37] A. Radford, J. Wu, R. Child, D. Luan, D. Amodei, I. Sutskever *et al.*, “Language models are unsupervised multitask learners,” *OpenAI blog*, vol. 1, no. 8, p. 9, 2019.
- [38] M. Rakowski, Y. Ban, P. De Heyn, N. Pantano, B. Snyder, S. Balakrishnan, S. Van Huylenbroeck, L. Bogaerts, C. Demeurisse, F. Inoue *et al.*, “Hybrid 14nm finfet-silicon photonics technology for low-power tb/s/mm² optical i/o,” in *2018 IEEE Symposium on VLSI Technology*. IEEE, 2018, pp. 221–222.
- [39] A. Shafaei, Y. Wang, X. Lin, and M. Pedram, “Fincacti: Architectural analysis and modeling of caches with deeply-scaled finfet devices,” in *2014 IEEE Computer Society Annual Symposium on VLSI*. IEEE, 2014, pp. 290–295.
- [40] Y. Shen, N. C. Harris, S. Skirlo *et al.*, “Deep learning with coherent nanophotonic circuits,” *Nature Photonics*, 2017.
- [41] M. Streshinsky, R. Ding, Y. Liu, A. Novack, Y. Yang, Y. Ma, X. Tu, E. K. S. Chee, A. E.-J. Lim, P. G.-Q. Lo *et al.*, “Low power 50 gb/s silicon traveling wave mach-zehnder modulator near 1300 nm,” *Optics express*, vol. 21, no. 25, pp. 30 350–30 357, 2013.
- [42] M. Sun, H. Ma, G. Kang, Y. Jiang, T. Chen, X. Ma, Z. Wang, and Y. Wang, “Vaqf: fully automatic software-hardware co-design framework for low-bit vision transformer,” *arXiv preprint arXiv:2201.06618*, 2022.
- [43] F. Sunny, A. Mirza, M. Nikdast, and S. Pasricha, “Crosslight: A cross-layer optimized silicon photonic neural network accelerator,” in *2021 58th ACM/IEEE Design Automation Conference (DAC)*. IEEE, 2021, pp. 1069–1074.
- [44] A. N. Tait, T. F. de Lima, E. Zhou *et al.*, “Neuromorphic photonic networks using silicon photonic weight banks,” *Sci. Rep.*, 2017.
- [45] E. Timurdogan, C. M. Sorace-Agaskar, J. Sun, E. S. Hosseini, A. Biberman, and M. R. Watts, “An ultralow power athermal silicon modulator,” *Nat Commun*, 2014.
- [46] H. Touvron, M. Cord, M. Douze, F. Massa, A. Sablayrolles, and H. Jégou, “Training data-efficient image transformers & distillation through attention,” in *International conference on machine learning*. PMLR, 2021, pp. 10 347–10 357.
- [47] A. Vaswani, N. Shazeer, N. Parmar, J. Uszkoreit, L. Jones, A. N. Gomez, Ł. Kaiser, and I. Polosukhin, “Attention is all you need,” *Advances in neural information processing systems*, vol. 30, 2017.
- [48] B. Wang, Z. Huang, W. V. Sorin, X. Zeng, D. Liang, M. Fiorentino, and R. G. Beausoleil, “A low-voltage si-ge avalanche photodiode for high-speed and energy efficient silicon photonic links,” *Journal of Lightwave Technology*, vol. 38, no. 12, pp. 3156–3163, 2019.
- [49] H. Wang, Z. Zhang, and S. Han, “Spatten: Efficient sparse attention architecture with cascade token and head pruning,” in *2021 IEEE International Symposium on High-Performance Computer Architecture (HPCA)*. IEEE, 2021, pp. 97–110.
- [50] M. Wang, S. Lu, D. Zhu, J. Lin, and Z. Wang, “A high-speed and low-complexity architecture for softmax function in deep learning,” in *2018 IEEE asia pacific conference on circuits and systems (APCCAS)*. IEEE, 2018, pp. 223–226.
- [51] C. Ye and D. Dai, “Ultra-compact broadband 2×2 3 db power splitter using a subwavelength-grating-assisted asymmetric directional coupler,” *Journal of Lightwave Technology*, vol. 38, no. 8, pp. 2370–2375, 2020.
- [52] H. You, Z. Sun, H. Shi, Z. Yu, Y. Zhao, Y. Zhang, C. Li, B. Li, and Y. Lin, “Vitcod: Vision transformer acceleration via dedicated algorithm and accelerator co-design,” in *2023 IEEE International Symposium on High-Performance Computer Architecture (HPCA)*. IEEE, 2023, pp. 273–286.
- [53] A. Zeng, X. Liu, Z. Du, Z. Wang, H. Lai, M. Ding, Z. Yang, Y. Xu, W. Zheng, X. Xia *et al.*, “Glm-130b: An open bilingual pre-trained model,” *arXiv preprint arXiv:2210.02414*, 2022.
- [54] S. Zheng, J. Zhang, and W. Zhang, “Scalable optical neural networks based on temporal computing,” *arXiv preprint arXiv:2303.01287*, 2023.
- [55] M. Zhou, W. Xu, J. Kang, and T. Rosing, “Transpim: A memory-based acceleration via software-hardware co-design for transformer,” in *2022 IEEE International Symposium on High-Performance Computer Architecture (HPCA)*. IEEE, 2022, pp. 1071–1085.
- [56] H. Zhu, J. Zou, H. Zhang, Y. Shi, S. Luo, N. Wang, H. Cai, L. Wan, B. Wang, X. Jiang *et al.*, “Space-efficient optical computing with an integrated chip diffractive neural network,” *Nature communications*, vol. 13, no. 1, p. 1044, 2022.